LANDMARK CONSTELLATION MATCHING FOR PLANETARY LANDER ABSOLUTE LOCALIZATION

Bach Van Pham, Simon Lacroix, Michel Devy
CNRS, LAAS, 7 Avenue du Colonel Roche, F-31077 Toulouse, France
University of Toulouse, UPS, INSA, INP, ISAE, LAAS, F-31077 Toulouse, France

Marc Drieux
EADS-ASTRIUM, 66 Route de Verneuil, Les Mureaux Cedex, 78133, France

Thomas Voirin
European Space Agency, ESTEC/ESA, Keplerlaan 1, Postbus 299, 2200 AG Noordwijk, The Netherlands

Keywords: Landmark Constellation, Pinpoint landing, Absolute navigation.

Abstract: Precise landing position is required for future planetary exploration missions in order to avoid obstacles on the surface or to get close to scientifically interesting areas. Nevertheless, the current Entry, Descent and Landing (EDL) technologies are still far from this capability, as the landing point is predicted with a dispersion of several kilometres. Therefore, research has been conducted to solve this absolute localization problem (also called "pinpoint landing"), which allows the spacecraft to localize itself within a known reference – namely orbital imagery. We propose an approach (nicknamed "Landstel") which relies on Landmark Constellation matching that gives an alternative to the current solutions and also avoids the drawbacks of existing algorithms. The fusion of the inertial sensor relative motion estimation and the Landstel global position estimation yields a better global position estimation and a higher system's robustness. Position estimation results obtained both with standalone Landstel and with the fusion of INS-Landstel via a simulator are shown and analysed.

1 INTRODUCTION

Precise landing position is required for future planetary exploration missions in order to avoid obstacles or to get close to scientifically interesting areas. Nevertheless, the current Entry, Descent and Landing (EDL) technologies are still far from this capability (Knocke et al., 2004). Therefore, much of research has been conducted to solve this absolute localization problem, referred to as "pinpoint landing", which allows the spacecraft to localize by itself within a known reference.

Several approaches have been introduced to solve the pinpoint landing problem using SIFT feature matching, crater detection and matching, or optic flow based approach (Trawny et al., 2006; Cheng and Ansar, 2005; Janscheck et al., 2006). Among these approaches, the VISINAV (Trawny et al., 2007) system can be considered as one of the most promising solution. The VISINAV system extracts surface landmarks in the descent image and then matches them to an ortho-rectified image of the scene. These matched points are then used either to estimate or update the spacecraft's position. The main drawback of the system is therefore its high memory requirement due to the storage of the scene image and the associated digital elevation map.

The absolute positioning system Landstel (Pham et al., 2009) is designed to cope with several constraints like low memory requirement, hardware implementation facility and illumination change robustness. Landstel uses a camera as its primary sensor, along with an altimeter and an inertial sensor – with which the lander is always equipped. Instead of using the image radiometric information, the Landstel system exploits the geometric relationship between point landmarks. Therefore, the Landstel system can work with varying illumination conditions, and especially match landmarks detected in the orbiter imagery and the lander images. The storage of individual landmarks (instead of the whole image) also reduces the

Van Pham B., Lacroix S., Devy M., Drieux M. and Voirin T. (2010).
LANDMARK CONSTELLATION MATCHING FOR PLANETARY LANDER ABSOLUTE LOCALIZATION.
In *Proceedings of the International Conference on Computer Vision Theory and Applications*, pages 267-274
DOI: 10.5220/0002815102670274

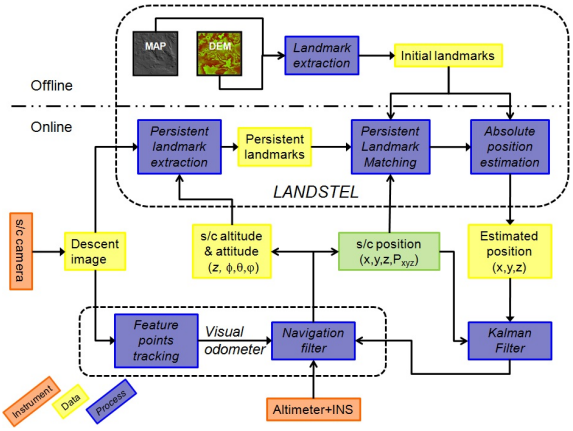

Figure 1: Overall navigation system architecture.

memory requirement for the system.

However, the performance obtained with Landstel in an "standalone" mode doesn't show the full potential of the whole navigation system (Pham et al., 2009). Therefore, this paper presents a coupling mode between Landstel and an INS to define a robust navigation solution. In this coupled system, the INS information is used to reduce and focus the search area for the Landstel system, and to compensate the position estimation error of Landstel via a complementary filter.

The next section presents the overall architecture in which the Landstel system is integrated. The various steps involved in the Landstel landmark matching algorithm are presented in section 3. Then, the paper presents the approach to fuse the absolute/global position estimated by Landstel with the relative movement estimated by the INS. Validation result obtained with standalone Landstel and with the Landstel-INS coupled system are presented in section 4.

2 OVERALL NAVIGATION SYSTEM DESCRIPTION

Figure 1 presents the overall navigation system architecture with three principle components: the visual odometer (*e.g.* like the NPAL camera (Astrium et al., 2006)) that also integrates INS data, the Landstel system and an external Kalman filter. The visual odometer, not described in this paper, provides an estimation of spacecraft's velocity and attitude.

The Landstel system is composed of one off-line and one on-line part. In the off-line part, the Digital Elevation Map (DEM) and the associated 2D ortho-image (MAP) of the foreseen landing area ($30km \times 30km$ for the current technology (Knocke et al., 2004)) are obtained on the basis of orbiter imagery. Initial visual landmarks are then extracted in the ortho-image (further denoted as the "geo-image"), using the Harris feature points detector (Harris and Stephens, 1988). Depending on the nature of the landing terrain, the appropriate visual landmarks are chosen. A signature is defined for each of the extracted feature points, according to the process depicted in section 3. The initial landmarks 2D position, their signature and their 3D absolute co-ordinates on the surface constitute a database stored in the lander's memory before launch.

On-line, the current altitude estimate is exploited to extract landmarks from the descent images (denoted as persistent landmarks in the figure), and the current spacecraft orientation estimate is used to warp the landmark coordinates, so as to enable matches with initial landmarks. Then, the spacecraft absolute position is fused via the Kalman filter with other available information provided by the visual odometer: speed, orientation, and previous absolute position estimation.

3 LANSTEL

3.1 Landstel Description

The Landstel algorithm consists in 5 steps (figure 2). The first and second steps extract and transform the information in the descent image so that the similarity between the descent landmarks and the initial landmark is maximized. Then, the third step is used to extract the signature of each descent landmark. The extracted signature of each descent landmark is compared with the initial landmarks signatures (step 4): to each descent landmark is associated a list of match candidates in the initial landmark set. In the last step, a voting scheme is applied to asses the correct matches: several affine transformations are extracted within the potential candidate list, and the best affine transformation (the one supported by the highest number of matches) is used to generate further matches between the descent image and the geo-image.

Step 1 - Landmark Extraction. Unlike the landmark extraction method used for geo-image, which is purely a Harris operator, the landmarks of the descent image are extracted with a scale adjustment operator (Dufournaud et al., 2002). The altimeter input is used to estimate the scale difference between geo-image and the descent image.

In fact, the scale-space associated with an image I can be obtained by convolving the initial image with a

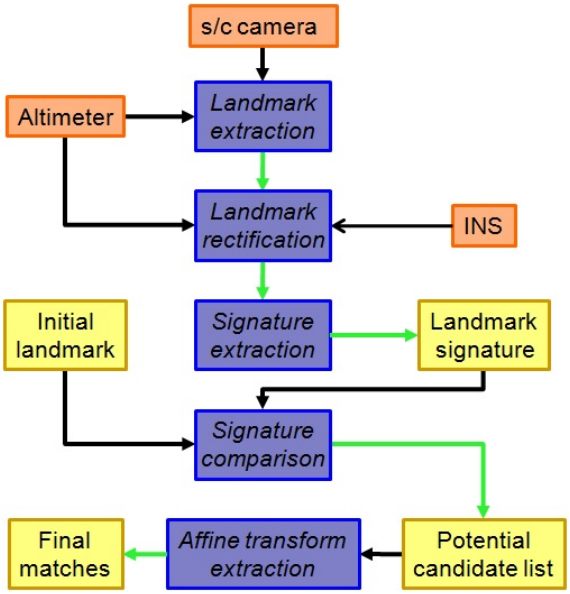

Figure 2: Landstel algorithmaArchitecture.

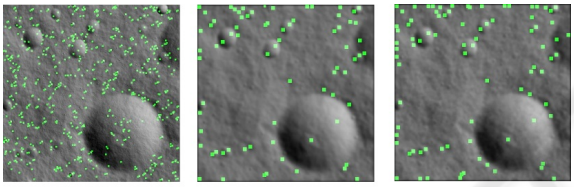

Figure 3: Landmarks detection with scale adjustment operator (a) Normal operator (b) Scale adjustment operator ($s = 3$) (c) Scale adjustment operator ($s = 4$) on the same image with added noise.

Gaussian kernel whose standard deviation is increasing monotonically, say $s\sigma$ with $s > 1$. In Figure 3, the two kinds of landmarks that are visible and invisible from a high altitude are detected in image (a), and only the ones that are visible from a high altitude are shown in image (b).

On the one hand, the scale adjustment operator helps to remove landmarks in the descent-image that have not been extracted in the geo-image. On the other hand, it filters the sensor noise thanks to the use of Gaussian kernel (see image (c) of figure 3, where the original image has been corrupted with a white noise $\mathcal{N}(0, 0.01)$, and with $s = 4$).

Step 2 - Landmark Rectification. Once extracted from the descent-image with the scale adjustment operator, the descent landmarks are warped to match the geo-image orientation with a homography transformation estimated with the spacecraft orientation provided by the inertial sensor (Figure 4, left). During this step, the landing zone is considered as a flat area due to the long distance between the spacecraft and the surface. This step will naturally ease the landmark matching process. Figure 4 right shows that after the scale adjustment operator and the image warping, the detected landmarks are pretty well matching those of the geo-image.

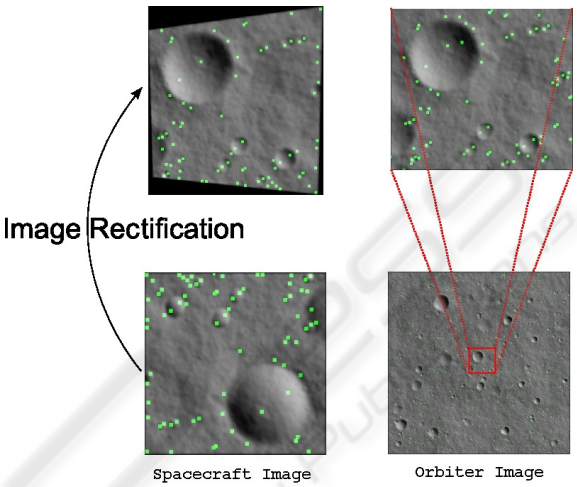

Figure 4: (a) Rectification of descent-image (b) Corresponding zoomed region in geo-image.

Step 3 - Signature Extraction. With the scale adjustment, the descent-landmarks have a pixel resolution similar to that of landmarks in the geo-image. The Landstel system uses this property to find matches between landmarks extracted from these two images: the signature of the landmark is indeed defined using their relative geometric repartition, measured using a variation of the Shape Context algorithm (Belongie and Malik, 2000).

The signature of a landmark L_i is extracted according to the following steps:

1. *Determination of Neighbors set*: a generic landmark L_j is added to the Neighbors set of L_i if and only if its pixelic distance to L_i, D_{ij}, satisfies the following condition

$$br < D_{ij} < pr \quad (1)$$

where br is the minimum distance which is used to prevent noise and pr is the pattern radius.

2. *Angular Distances Discretization and Sector Discretization*: the landmarks pixelic distances and their angular values in the Neighbors set of L_i are then discretized into a bi-dimensional $nRings \times nWedges$ array, corresponding to $nRings$ rings centered on L_i and to $nWedges$ sectors (figure 5). An occupancy histogram, normalized into a probabilistic distribution, defines the signature.

As a result, a landmark signature is a bi-dimensional vector of $nRings \times nWedges$ bytes.

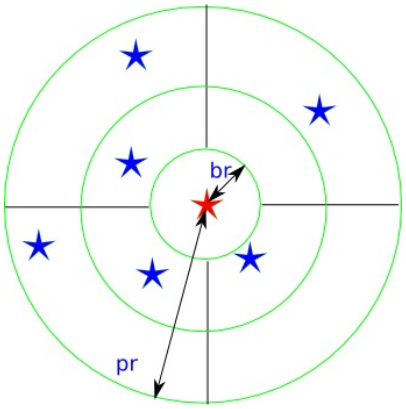

Figure 5: Discretisation used to compute the landmark signature.

Step 4 - Signature Comparison. In order to calculate the similarity between two landmarks g and k, the Chi-Square distance C_{gk} is used:

$$C_{gh} = \frac{1}{2}\sum_{k=1}^{k}\frac{[g(k)-h(k)]^2}{g(k)+h(k)} \quad (2)$$

Any pair of landmarks whose distance is smaller than a threshold is considered as a potential match, which defines for each descent landmark L_i a list of potential geo landmark matches.

Step 5 - Affine Transformation Estimation. Given the candidate lists obtained with the previous steps, several affine transformations between the descent-image the geo-image are calculated, each affine transformation defning a number of matches.

The main process used in this step is the interpretation tree and the vector distance metrics. Given two match pairs (L_i, K_i) and (L_j, K_j) where L and K respectively represent the descent and geo landmarks, these pairs are considered as consistent if and only if their vector distance $distVector([L_i, L_j], [K_i, K_j])$, defined as the difference between the two vectors lengths and orientations, is smaller than a predefined threshold ε. This vector distance is meaningful because the two landmark sets share the same coordinate system after the application of the affine transformation (the translation component is not considered in the vector distance).

On the basis of the vector distance metrics, an affine transformation (estimated with at least 3 matches) can be estimated by searching an interpretation tree formed with the candidates lists. If an affine transformation is found, the associated matches are stored aside. Other new affine transformations are searched using remaining other candidates in the potential candidate list.

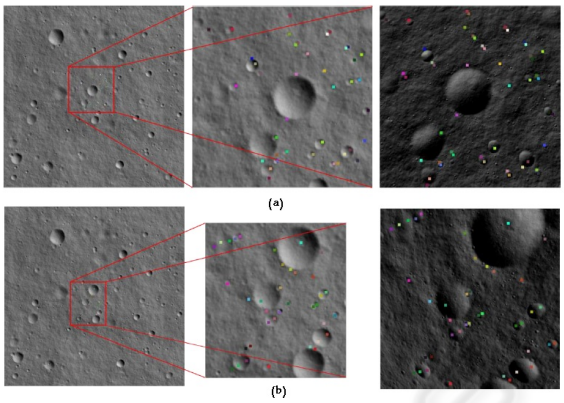

Figure 6: Two examples of matches established by Landstel under different illumination conditions.

For each estimated affine transformation, the number of matches between the descent landmarks and geo-landmarks are calculated. The affine transformation with the highest number of matches is used to generate the final matches between the two images. If the number of matches is greater than a pre-defined threshold, the found final matches are considered as correct and used to estimate the absolute spacecraft's position.

3.2 Landstel Illustration

Figures 6 shows two examples of the final matches with different illumination conditions. The geo-image (left) is acquired with 55-25 (azimuth-elevation) sun position, whereas the descent images (right) are acquired at 5710m altitude with 145-10 Sun position (a) and at 3052m altitude with 235-10 Sun position (b). The center images show the corresponding matched regions of the descent-images in the geo-images.

3.3 Absolute Spacecraft Position Estimation

Given a set of matches between the descent image and the geo-image, the spacecraft's position can be estimated using the image projection function as illustrated in Figure 7:

1. The landmarks 2D positions (U) in the descent image
2. The landmarks 3D positions (M) in the landing zone (deduced through their matches with the geo-image) expressed in a known coordinates frame

3. The image projection function:

$$U = K[R^T, -R^T T]M \tag{3}$$

where K is the 3×3 intrinsic matrix of the camera, R the image rotation (provided by the navigation filter) and T the spacecraft position[1] (Figure 7).

Knowing U, K, R and M, the spacecraft position T can be calculated using a non-linear optimization algorithm.

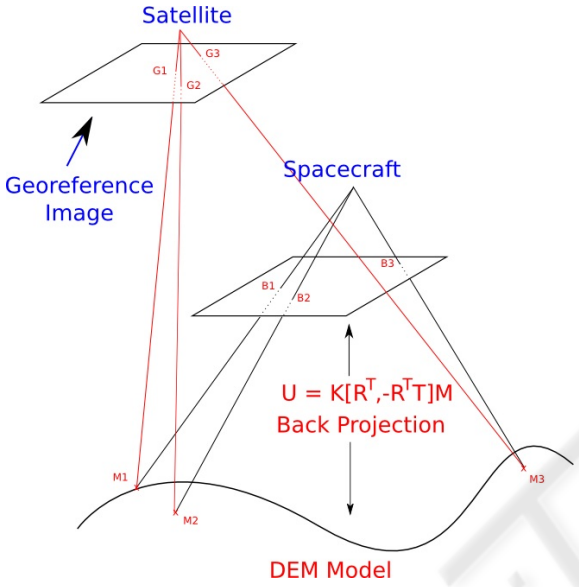

Figure 7: Spacecraft position estimation.

4 KALMAN FILTER DESCRIPTION

The main objective of fusing the Landstel absolute position estimates with the relative motion estimates provided by the INS (or the visual odometry block of figure 1) is to yield a more precise abolsute estimate of the spacecraft position. This is achieved thanks to a complementary filter (a Kalman filter in this case, set up as shown in Figure 8).

But in turn, the integration of the estimated motions provided by the INS sensor can help Landstel, by focusing the match search within a specific region of the geo-image instead of searching in the whole landing area, as when using Landstel in a standalone mode. This focusing mechanism not only accelerates the algorithm by reducing the search area, but also improves the algorithm's performance by limiting the false matches probability.

[1]For simplification purpose, the spacecraft reference frame is assimilated to the camera one here.

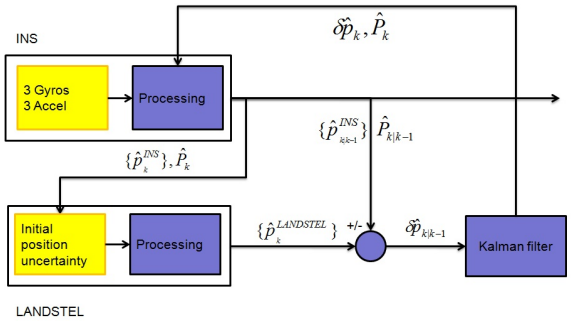

Figure 8: The Landstel-INS fusion principle.

4.1 Kalman Filter Structure

The Kalman filter setup presented in figure 8 is the following:

1. System state:

$$x = [\delta\Psi^T \delta v^T \delta p^T] \tag{4}$$

where $\delta\Psi$ is the system attitude error, δv the system speed error and δp the system position error. Each of these is a 3-dimensional vector (3×1). In this case, the control value is equal to zero : $u = 0$.

2. Transition matrix:

$$\Phi_k = \begin{bmatrix} -\Omega^e_{ie} & 0_3 & 0_3 \\ [a\times] & -2\Omega^e_{ie} & \Upsilon \\ 0_3 & I_3 & 0_3 \end{bmatrix} \tag{5}$$

where Ω^e_{ie} is a skew-symmetric matrix which represents the planet rotation given by the angular rate $\omega^e_{ie} = [\omega_1, \omega_2, \omega_3]$ between the planet-centered inertial frame (i-frame) and the planet-centered planet-fixed frame (e-frame):

$$\Omega^e_{ie} = \begin{bmatrix} 0 & -\omega_3 & \omega_2 \\ \omega_3 & 0 & -\omega_1 \\ -\omega_2 & \omega_1 & 0 \end{bmatrix} \tag{6}$$

and $\Upsilon = -(\Omega^e_{ie}\Omega^e_{ie} - \Gamma^e)$, Γ^e being the short notation for the gravity gradient (the derivative of the gravity). The 0_3 symbol denotes a 3×3 matrix while a I_3 denotes a 3×3 identity matrix. The $[a\times]$ represents the misalignment of the transformation matrix between the i-frame and the e-frame.

3. Observation state: the observations from the Landstel system are only the spacecraft position. Hence when a Landstel absolute position estimation becomes available, an error observation is obtained, and the filter then updates the estimate of the error states in the INS. Otherwise, the system can use the inertial sensor alone to navigate.

$$z_k = \begin{bmatrix} 0_{2\times 3} \\ [p_k^{INS} - p_k^{Landstel}] \end{bmatrix} \quad (7)$$

4. Observation matrix:

$$H_k = \begin{bmatrix} 0 & 0 & 0 \\ 0 & 0 & 0 \\ 1 & 1 & 1 \end{bmatrix} \quad (8)$$

4.2 Kalman Filter Design

As the Kalman filter used in the navigation system is a feed backward filter where the estimated error is provided to the INS after each observation, the prediction state in this case is always equal to zero. In fact, initially the inertial sensors are considered as being calibrated and all the errors are removed, thus the prediction state $x(1|0)$ is set to zero. Moreover, after each estimation with the Kalman filter, the estimated error is always returned back to the INS sensor for correction due to the feed backward Kalman filter. As a consequence, the error in the INS sensor is considered as being corrected which results in a zero prediction state.

The interests of the Kalman filter in this case are firstly to estimate the error in the estimated position provided by the INS and also by the previous Kalman update via the feed backward mechanism. The second goal of the Kalman filter is to estimate the uncertainty in the estimated position. The uncertainty of the estimated position can be evaluated through the predicted covariance matrix $\hat{P}_{k|k-1}$.

5 RESULTS

5.1 Experiment Profile

The Landstel landmarks matching algorithm has been tested with the PANGU simulator v2.7 (Parkes et al., 2004). In this experiment, a simulated trajectory of a spacecraft during its Mars entry phase is used, from the early parachute phase to the end of the powered guidance phase. The spacecraft begins its image acquisition at 8 km altitude with 30 degree inclination (with respect to the vertical axis) and with a speed of $500m/s$. The initial position uncertainty is $15 \times 15km^2$. At 2 km altitude, the spacecraft becomes parallel with the vertical axis with 0 degree inclination. Then, a propulsion system is used to land the spacecraft to the ground during 38 seconds. In total, the whole descent process will take about 65 seconds from the beginning of the parachute phase to the final touch down. Therefore, there are 65 images taken for each trajectory at 1Hz sample rate.

In order to generate more trajectories for the validation process, the simulated trajectory is rotated 30 degrees in the X-Y plane. By this way, 12 different trajectories are generated. These 12 trajectories begin the parachute phase at different places and with different angles. The common point of these trajectories is that they always land the spacecraft in the center of the image[2].

The simulated terrain is a heavily craterized surface with about 20 $craters/km^2$ and has a surface of $32 \times 32km^2$.

The descent-image is compared to the geo-image with multiple resolutions as shown figure 9. Since the spacecraft approaches the surface, the coarseness of the acquired image is reduced as shown in the right image. In order to ensure the highest correlation between the descent-image and the geo-image, the geo-image layer is changed with respect to different instances as shown in Figure 9. The altitudes a which the geo-image resolution is switched are predefined.

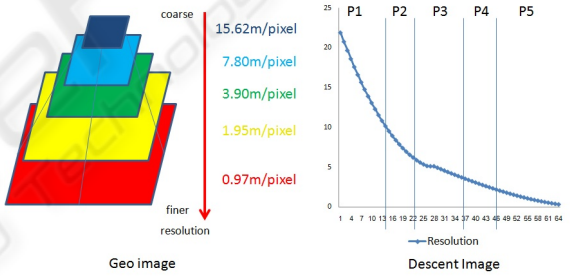

Figure 9: Multi-resolution geo-image.

Since the geo-image is taken under illumination conditions which can be different from the conditions as the spacecraft descends, different illumination conditions are used to verify the robustness of the system. Here, the geo-image illumination condition is fixed to 0-5 degrees azimuth-elevation. The conditions during the spacecraft descent vary as indicated in table 1. The first number is each bracket is the azimuth value which is an increment of 40 degrees and the second number indicates the elevation value which is either 1 degree or 10 degrees. Therefore, there are 18 different illumination conditions used. In summary, the 18 different illuminations combined with the 12 different trajectories generate 216 test cases (or "trials"),

[2]This is due to the way Pangu handles large terrain models – the higher resolution being only available in the center of the model.

i.e. 14040 images in total[3].

Table 1: Descent image illumination conditions.

(00,01)	(40,01)	...	(280,01)	(320,01)
(00,10)	(40,10)	...	(280,10)	(320,10)

In order to verify the robustness of the system with different levels of sensor noise, the experiment is set up with the following configuration:

1. Image: white noise $\mathcal{N}(0, 0.005)$
2. Radar altimeter: 2.5 percent of measured distance (e.g. 5000m altitude with $\pm 125m$ error).
3. Attitude noise: the INS is considered as extremely precise due to the short landing time and the usage of the visual odometer (standard deviation well below 1° – the Landstel has however shown to be able to cope with 5° attitude angle errors (Pham et al., 2009)).

5.2 System Performance

5.2.1 Overall Performance

Figure 10 shows the estimation results obtained. As shown in the two charts, the combination of the inertial sensor and the Landstel system shows better performance than Landstel in a standalone mode. In this case, the number of "no estimation" is decreased from 26 percent down to 19 percent. Moreover, the number of "false estimations" is also decreased from 3 percent down to less than 1 percent (105 false estimations in 14040 cases). As a consequence, the number of correct estimations is increased from 71 percent up to 80 percent. Concerning the false estimations delivered by the INS-Landstel fusion, most of the cases happen at the end of each geo-image layer transition where the correlation between the descent image resolution and the geo-image layer becomes weak.

5.2.2 Localization Performance

In general, from the initial 15×15 km^2 uncertainty, both of the standalone Landstel and the INS-Landstel systems can localize the spacecraft's position with a precision below 10×10 m^2 at the final touch down. However, the difference between the two systems is the number of false position estimations which can severely influence the whole spacecraft's performance.

[3]Dozens of similar tests with different terrain configurations, yieding the same number of images, have also been evaluated.

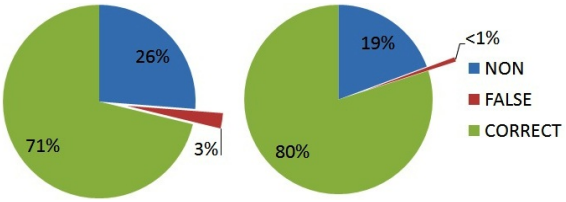

Figure 10: Estimation result with the number of "False" and "correct" estimations, and the number of images where the algorithm can not find matches. The left chart shows the results obtained with Landstel in a standalone mode, the right one shows the result obtained with INS-Landstel fusion.

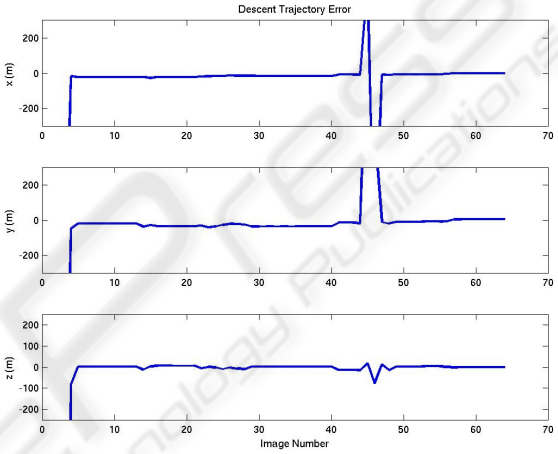

Figure 11: Estimation error with standalone Landstel.

Figure 11 shows for one trial the difference between the the estimated position returned by standalone Landstel and the true spacecraft trajectory. The sun condition in this trial is 180 degrees in azimuth and 1 degree in elevation for the descent-image.

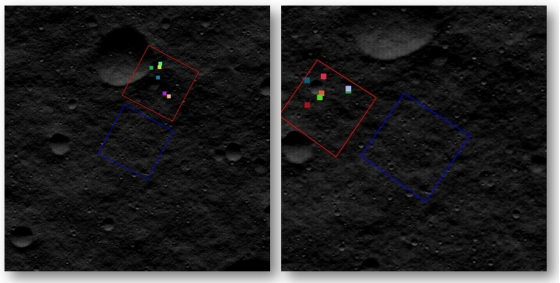

Figure 12: Two false position estimations situations with standalone Landstel. The red zone indicates the estimated the spacecraft's camera's field of view, whilst the blue zone indicates the true spacecraft's camera's field of view.

In this trial, the standalone Landstel system returns two false estimations which occur at the 45^{th} and the 46^{th} images, which results in two big error jumps as shown in Figure 11. The two erroneous

cases are shown in Figure 12. In this Figure, the shown images are the cropped zones of the geo-image in order to enhance the visibility. However, the images' intensity is not changed so as to reflect the true illumination condition of the geo-image.

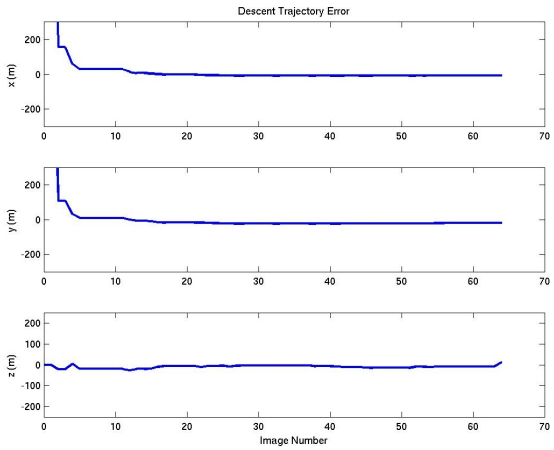

Figure 13: Estimation error with the INS-Landstel fusion.

In contrast, with the same trial, the INS-Landstel fusion can avoid these two errors as shown in Figure 13. With the motion estimation of the inertial sensor, the research zone within the geo-image is well focused, which reduces the probability of false matching occurrences.

6 CONCLUSIONS

In this paper, we have demonstrated the ability of a vision-based algorithm coupled with the inertial sensor for spacecraft absolute localization with respect to an orbiter image. Similarly to an INS-GPS fusion problem, the advantages obtained are twofold. Firstly, the localization precision is higher. Secondly, the research zone within the geo-image for the Landstel algorithm is greatly reduced, which both enhances the algorithm's speed and reduces the probability of false matches.

However, the fusion mechanism introduced in this paper only exchanges the position (both global and relative) information of the two sensors. A tighter integration of the two sensors with respect to the interest points detected by both sensors is currently being analysed and evaluated. First results have shown a promising application of this type of integration.

REFERENCES

Astrium, E., Avionica, G., of Dundee, U., INETI, and SCISYS (2006). Navigation for planetary approach & landing. *ESA Contract*.

Belongie, S. and Malik, J. (2000). Matching with shape context. *IEEE Workshop on Context Based Access of Image and Video Libraries*.

Cheng, Y. and Ansar, A. (2005). Landmark based position estimation for pinpoint landing on mars. *Proceedings of the 2005 IEEE International Conference on Robotics and Automation*, pages 1573 – 1578.

Dufournaud, Y., Schmid, C., and Horaud, R. (2002). Image matching with scale adjustment. *INRIA Report*.

Harris, C. and Stephens, M. (1988). A combined corner and edge detector. *Proceedings of the 4th Alvey Vision Conference*.

Janscheck, K., Techernykh, V., and Beck, M. (2006). Performance analysis for visual planetary landing navigation using optical flow and dem matching. *AIAA Guidance, Navigation and Control*.

Knocke, P. C., Wawrzyniak, G. G., Kennedy, B. M., and Parker, T. J. (2004). Mars exploration rovers landing dispersion analysis. *AIAA/AAS Astrodynamics Specialist Conference and Exhibit*.

Parkes, S., Martin, I., Dunstan, M., and Matthews, D. (2004). Planet surface simulation with pangu. *SpaceOps*.

Pham, B. V., Lacroix, S., Devy, M., Drieux, M., and Philippe, C. (2009). Visual landmark constellation matching for spacecraft pinpoint landing. *AIAA Guidance, Navigation and Control*.

Trawny, N., Mourikis, A. I., and Roumeliotis, S. I. (2007). Coupled vision and inertial navigation for pin-point landing. *NASA Science Technology Conference*.

Trawny, N., Mourikis, A. I., Roumeliotis, S. I., Johnson, A. E., and Montgomery, J. (2006). Vision-aided inertial navigation for pin-point landing using observations for mapped landmarks. *Journal of Fields Robotics*.